Prepared for submission to JHEP

Can Tonne-Scale Direct Detection Experiments Discover Nuclear Dark Matter?

Alistair Butcher, Russell Kirk, Jocelyn Monroe and Stephen M. West

Dept. of Physics, Royal Holloway University of London, Egham, Surrey, TW20 0EX, U.K.

E-mail: Alistair.Butcher.2010@live.rhul.ac.uk, Russell.Kirk.2008@live.rhul.ac.uk, Jocelyn.Monroe@rhul.ac.uk, Stephen.West@rhul.ac.uk

Abstract: Models of nuclear dark matter propose that the dark sector contains large composite states consisting of dark nucleons in analogy to Standard Model nuclei. We examine the direct detection phenomenology of a particular class of nuclear dark matter model at the current generation of tonne-scale liquid noble experiments, in particular DEAP-3600 and XENON1T. In our chosen nuclear dark matter scenario distinctive features arise in the recoil energy spectra due to the non-point-like nature of the composite dark matter state. We calculate the number of events required to distinguish these spectra from those of a standard point-like WIMP state with a decaying exponential recoil spectrum. In the most favourable regions of nuclear dark matter parameter space, we find that a few tens of events are needed to distinguish nuclear dark matter from WIMPs at the $3\,\sigma$ level in a single experiment. Given the total exposure time of DEAP-3600 and XENON1T we find that at best a $2\,\sigma$ distinction is possible by these experiments individually, while $3\,\sigma$ sensitivity is reached for a range of parameters by the combination of the two experiments. We show that future upgrades of these experiments have potential to distinguish a large range of nuclear dark matter models from that of a WIMP at greater than $3\,\sigma$.

Contents

1 Introduction

A large body of indirect evidence has strongly motivated the existence of dark matter; non-baryonic matter constituting approximately a quarter of the Universe's energy density [1]. In order to fully explain dark matter, we are compelled to consider Beyond the Standard Model (BSM) theories as the Standard Model (SM) is incapable of accounting for all of the dark matter energy density. Most BSM theories assume that dark matter takes the form of (or at least interacts as) point-like particles, but this is not necessarily the case. The SM already provides a clear example of a more complicated structure with normal matter existing in a rich spectrum of composite states. We are therefore motivated to ask whether a similar structure exists in the dark sector and whether this leads to important phenomenological consequences.

The idea that the dark matter states in our Universe are not point-like is not new, for example the formation of bound states of two WIMP particles was considered in [2–4], and a recent analysis has examined the generic direct detection phenomenology of these WIMPonium states [5, 6]. It is also possible to build dark analogues of simple SM atoms[1], for example dark Hydrogen [14], consisting of a bound state formed between a dark proton and a dark electron. This idea has also been extended to the case of dark molecular objects leading to interesting limits on their atomic properties from constraints on their self-scattering cross-sections [15, 16].

This paper focuses on the possibility of nuclear dark matter (NDM), where dark matter is composed of bound states of strongly-interacting dark nucleon (DN) constituents

[1]For related and earlier attempts to explain dark matter using a SM analogue see for example [7–13].

with short-range interactions [17–22]. In particular, we will consider the class of dark nuclei outlined in [21, 22] focussing on the potential signals in (and constraints from) direct detection experiments. This class of model assumes that the dark nuclei have an approximately uniform density, with a hard core repulsion between the constituent DNs. This is in contrast to the dark matter "nuggets" described in [19, 20], where no hard core repulsion was assumed resulting in a more complicated internal structure.

In comparison to standard WIMP dark matter, the mass of a typical dark nucleus can be much larger. For example, in [21, 22] dark nuclei with a large number of constituents each with masses in the GeV region were considered leading to states with a total mass well in excess of the unitarity limit of thermal WIMP dark matter.

The composite and extended nature of these dark matter states will affect the way in which they scatter off SM nuclei in direct detection experiments. If all dark matter is in the form of composite states each with k dark nucleons (which we refer to as a k-DN state), and if the momentum transfer in the scattering process is less than the inverse radius of the state then the elastic scattering cross-section will be coherently enhanced by a factor of k^2 [17, 21–23]. However, as we increase k the number density of these k-DN states will decrease, leaving an overall event rate increasing linearly with k [22].

The dependence of the scattering rate on the spatial properties of both the extended dark matter states and the SM nuclei is encoded in the product of their respective form factors. These form factors are as usual related to the Fourier transforms of the spatial densities of the particular composite object. If the radii of the dark matter states are larger than the SM nuclei, off which they are scattering, then direct detection experiments will start to probe the dark form factor at lower values of the momentum transfer compared to the SM form factor. This can lead to a striking structure in the recoil spectrum [22]. For example, if we assume that the composite dark matter states possess a uniform internal density, and model this density in terms of a spherical top hat function, the resulting form factor is a spherical Bessel function. The recoil energy spectrum will as a result include characteristic peaks and troughs. Whether these features are distinguishable depends upon the individual experiment's energy resolution and threshold, and is the focus of this work.

The appearance of these distinctive peaks and troughs in the recoil spectrum also depends on whether all dark matter states have the same number of DNs or whether there is a distribution of nuclei with different k values. The position of the troughs and peaks in the recoil spectrum is dependent on the value of k and it was shown in [22] that the compound recoil spectrum from a distribution of k values results in the peaks and troughs being smoothed out leaving a monotonically decreasing spectrum. While more difficult, in a single detector with a sufficiently high number of signal events the recoil spectrum in this case may still be distinguishable from that of a standard WIMP for a given dark matter velocity distribution. Due to the uncertainty in the dark matter velocity distribution a more effective way to distinguish between NDM and WIMP spectra is to perform a halo-independent analysis using data from several different detectors (see for example [24]). In this paper however we wish to study the simpler case of dark nuclei existing predominantly with a fixed number of DNs leaving the halo-independent analysis for future work.

In [22] a simplified direct detection analysis of fixed k dark nuclei was performed using

approximations of future detectors. In this paper we build on this work and perform an in-depth analysis of NDM at DEAP-3600 [25] and XENON1T [26] using the predicted detectors' energy response functions, efficiencies and thresholds.

The first detector we consider is the liquid argon detector DEAP-3600, which will soon begin its 3 year run and will be roughly an order of magnitude more sensitive to the WIMP scattering cross-section than current searches at a 100 GeV WIMP mass. We have chosen DEAP-3600 as one of our test cases as it has excellent energy resolution, which will be important if we hope to be able to identify peaks and troughs in the recoil energy spectrum. DEAP-3600 also has a better sensitivity to high mass dark matter states due to the slow (compared to xenon) fall off in the argon nuclear form factor.

The second direct detection experiment XENON1T is a liquid xenon detector which will also soon begin its physics run, and will be roughly two orders of magnitude more sensitive to the WIMP scattering cross-section than current searches in the mass range of 10-50 GeV. The use of the xenon target allows for a few-keV energy threshold, potentially giving sensitivity to features in the recoil energy spectrum at the lower energies where the scattering rate is largest.

Although our focus is to analyse the potential distinguishability of NDM from a standard WIMP signal, this paper includes an analysis of the current and future constraints on NDM if no signal is observed. We use the limits on WIMP dark matter from LUX [27] to calculate the current upper bounds on the DN-SM nucleon scattering cross-section for fixed k dark nuclei and go on to calculate the potential future limits arising from DEAP-3600 and XENON1T.

Following this introduction, in Section 2 we outline our chosen model of NDM and review the calculation of the recoil spectrum. In Section 3 we detail the specifications of DEAP-3600, XENON1T, and LUX, including the predicted energy resolutions, efficiencies, and energy thresholds used in our analyses. We go on to explore the generic features of the recoil energy spectra for a selection of benchmark NDM scenarios at DEAP-3600 and XENON1T, detailing the effect of the energy resolution and energy threshold on the observability of the features produced by dark form factors. We then present the current and projected (if no signals are observed) limits on NDM from LUX and the two tonne-scale direct detection experiments respectively. In Section 4 we turn to the main component of this work, calculating the number of signal events required in order to distinguish a NDM spectrum from a decaying exponential recoil spectrum produced by a WIMP. In light of this analysis we discuss the potential for the discovery of NDM at DEAP-3600 and XENON1T. Finally we discuss our results and conclude in Section 5.

2 Nuclear Dark Matter Recoil Spectrum

The scenario we consider here is a variant of the general class of model described in [21], where dark nuclei generically exist in a wide distribution of sizes. The assumptions of [21] include the existence of a binding energy per DN that saturates (rather than turning over) at large dark nucleon number leading to fusion processes that continue to produce larger and larger dark nuclei with the limit in size being determined by the temperature at

which the fusion processes freeze-out. This results in a distribution over different sizes of dark nuclei. In this case, the predicted peaks and troughs in the recoil spectrum expected for a single size of dark nucleus are washed out when the cumulative effect of the wide distribution over k is taken into account [22].

The modified case where the distribution of dark nuclei sizes are focused around a particular value of k can in principle arise if the binding energy per DN turns over at some nucleon number, in the same way the SM nuclear binding energy per nucleon does at iron. This turnover, for example, could arise in the dark sector in an analogous way to the SM by introducing a dark equivalent of the coulomb force. The direct detection prospects of this scenario is qualitatively different to that of the wide distribution and deserves detailed attention. This is the scenario we consider here, *i.e* the present dark matter abundance is assumed to consist entirely of dark nuclei with same number of DNs. Given the structure in the recoil spectrum for our chosen case, it is likely that this scenario would be the easiest to identify and hence is a sensible case with which to start.

In this analysis we will consider the underlying interaction between the DNs and SM quarks being due to the exchange of a heavy scalar mediator. The elastic scattering rate of two spatially extended states will then depend on the product of the respective form factors derived from the Fourier transforms of the individual spatial densities of the colliding objects.

The composite dark matter states we consider have an approximately uniform density of constituent matter and we model the density as a spherical top hat function, leading to a spherical Bessel function form factor,

$$F_k(q) = \frac{3j_1(qR_k)}{qR_k}, \tag{2.1}$$

where R_k is the radius of the dark mater state and q is the momentum transfer in the collision. Under the assumption of a constant density and negligible binding energy, the radius of a k-DN state is approximated by

$$R_k = k^{1/3}R_1, \tag{2.2}$$

where R_1 is the approximate radius of a single DN.

For the SM nuclear form factor, we use the Helm parameterisation [28]

$$F_N(q) = \frac{3j_1(qR_N)}{qR_N}e^{-q^2s^2/2}, \tag{2.3}$$

which represents a modification to the spherical top hat density to include a finite-width drop off with skin depth $s = 0.9$ fm. For the SM nuclei's radius R_N, we employ the approximate analytic expression

$$R_N^2 = c^2 + \frac{7}{3}\pi^2a^2 - 5s^2, \tag{2.4}$$

with $c \approx 1.23A^{1/3} - 0.6$ fm (where A is the SM nucleon number), and $a = 0.52$ fm [29].

The recoil spectrum, that is, the differential scattering rate per unit target mass for a dark matter particle (whether a WIMP, NDM state, or otherwise) to scatter off a SM nucleus, is given by

$$\frac{dR}{dE_R} = \frac{1}{m_N} \int_{v>v_{\min}} d^3\mathbf{v}\ \frac{\rho_X}{m_X} f(\mathbf{v}) v \frac{d\sigma_{XN}}{dE_R}\bigg|_v, \tag{2.5}$$

where $v_{\min} = \sqrt{\frac{E_R m_N}{2\mu_{XN}^2}}$ (for non-relativistic scattering) is the minimum velocity required to obtain a recoil energy E_R, μ_{XN} is the reduced mass of the SM nuclei-dark matter state system, σ_{XN} is the SM nuclei-dark matter scattering cross-section, ρ_X is the local dark matter density, m_N and m_X are the masses of the SM-nucleus and dark matter state respectively, and $f(\mathbf{v})$ is the dark matter velocity distribution.

Now specifying to our case of a NDM state with k dark nucleons we follow [21] and assume that the underlying scattering process between the SM and DNs is isotropic and velocity-independent. This allows us to write the differential event rate as

$$\frac{dR}{dE_R} = g(v_{\min}) \frac{\rho_k}{2\mu_{kn}^2 m_1} A^2 k \sigma_0 F_N(q)^2 F_k(q)^2, \tag{2.6}$$

where σ_0 is defined as the zero-momentum transfer DN-SM nucleon scattering cross-section (and so $F_k(0) = F_N(0) = 1$), μ_{kn} is the reduced mass of the DN-SM nucleon system, m_1 is the mass of a single DN, $q = \sqrt{2 m_N E_R}$, and

$$g(v_{\min}) = \int_{v>v_{\min}} d^3\mathbf{v} \frac{f(\mathbf{v})}{v}. \tag{2.7}$$

Note that the event rate is proportional to a linear factor of k due to the cancellation of one power of the coherence factor (k^2) with a power of k in the denominator coming from the mass of the dark nuclear state, $m_k = k m_1$. As we will only consider the case of a single size of dark nuclei, the density of k-DN states, ρ_k, is the total local dark matter density.

In order to determine the recoil spectrum reconstructed by an experiment, one must take into account the detector's efficiency $\epsilon_{\text{eff}}(E_R)$, and energy resolution $\sigma(E_R)$. The reconstructed recoil spectra are then found using

$$\begin{aligned} \frac{dR_{\text{rec}}}{dE_R} &= \int dE'_R \epsilon_{\text{eff}}(E'_R) \kappa(E_R, E'_R) \frac{dR}{dE'_R} \\ &\approx \int dE'_R \frac{\epsilon_{\text{eff}}(E'_R)}{\sqrt{2\pi}\sigma(E'_R)} \exp\left(-\frac{(E_R - E'_R)^2}{2\sigma^2(E'_R)}\right) \frac{dR}{dE'_R} \end{aligned} \tag{2.8}$$

where $\kappa(E_R, E'_R)$ is the energy response function, which we have taken to be a Gaussian.

The predicted number of events seen by a detector is then

$$N = \left(\int_{E'_{\text{low}}}^{E'_{\text{up}}} dE_R \frac{dR_{\text{rec}}}{dE_R} \right) \times \text{Exposure}, \tag{2.9}$$

where E'_{low} and E'_{up} are the limits of the reconstructed energy window used in the analysis, and the exposure is the fiducial mass of the detector multiplied by its livetime.

3 Nuclear Dark Matter in Tonne-Scale Direct Detection Experiments

3.1 Energy Resolutions, Efficiencies and Energy Windows.

In this section we detail the parameterisation of the predicted energy resolution, detector efficiency and recoil energy window used in our analysis for each experiment we consider. The recoil energy spectrum, Equation (2.1), has two features that play an important role in the analysis. The first is the oscillatory nature of the Bessel function leading to non-decreasing sections of the recoil spectrum. In order to identify these features the experiment needs to have sufficiently good energy resolution. For this reason we have included an analysis with DEAP-3600, which has a particular focus on maximising the detected yield per unit of deposited energy (photoelectrons per keVee) and electronics designed to give excellent resolution over orders of magnitude in dynamic range, thereby producing a leading energy resolution.

The second important feature of the NDM recoil spectrum is that the first few peaks at low energy dominate the event rate. This means that a low recoil energy threshold is an advantage for maximising the event rate. In addition, for large k states the frequency of oscillations is higher and so in order to distinguish between NDM and WIMP models we need to detect as many events as possible in the non-decreasing part of the spectrum, motivating the lowest possible recoil energy threshold. For this reason, we have included an analysis with XENON1T, which combines a low recoil energy threshold with tonne-scale fiducial mass.

The size of the full signal energy window and the efficiency within the window for each experiment also plays a role in determining how many of the NDM form factor oscillations are in principle observable in each experiment. We start with the details of DEAP-3600.

DEAP-3600 is a single-phase scintillation detector with a 1000 kg fiducial mass target of liquid argon, which will begin its search in the near future and results are anticipated over the next few years. In the single-phase detector, an array of photomultiplier tubes (PMTs) views the target over the full solid angle of 4π to detect the scintillation light of any possible dark matter scatterings. This approach maximises the number of photoelectrons (PE) detected, which is a function of the recoil energy (in keV) imparted by the collisions. To predict how WIMPs and NDM will be reconstructed we ran Monte Carlo simulations of $\sim 8 \times 10^6$ events in a DEAP-like detector simulation, with parameters drawn from [25]. The energy resolution and efficiency were then found by fitting functions to the resulting distributions of measured PE versus generated recoil energy resulting in

$$\begin{aligned} \sigma(E_R) &= 0.54\,\text{keV}\sqrt{E_R/\text{keV}} - 0.048\,\text{keV}(E_R/\text{keV}) + 0.0026\,\text{keV}(E_R/\text{keV})^{3/2}, \\ \epsilon(E_R) &= 0.56\,\text{erf}(0.044\ E_R/\text{keV}). \end{aligned} \tag{3.1}$$

We consider events in a recoil energy range of approximately $20 < E_R < 120$ keV (in fact selecting events with $50 < E_R < 300$ detected PE), since below this there are not enough PEs to accurately reconstruct the position of the event, and above there are too few dark matter scatters.

XENON1T is a two-phase scintillation detector with 1000 kg fiducial mass of liquid xenon target. XENON1T is currently in the commissioning phase and will begin its physics

run shortly. The relevant information for XENON1T was taken from [26], with an approximation for the energy resolution given by [30]. This and the efficiency were then taken to be

$$\begin{gathered}\sigma(E_R) = -0.47\,\mathrm{keV} + 0.65\,\mathrm{keV}\sqrt{E_R/\mathrm{keV}} + 0.02\,\mathrm{keV}(E_R/\mathrm{keV}), \\ \epsilon(E_R) = 0.4,\end{gathered} \tag{3.2}$$

where the energy window $4 < E_R < 50\,\mathrm{keV}$ is used.

We also calculate the bound on NDM from the existing published LUX results [27]. All requisite information for LUX, apart from the energy resolution, was taken from a recent improved analysis of the 2013 data [27] and the first results report [31]. For the energy resolution, we use the resolution for electron recoils from a more recent calibration of LUX using tritium decays [32], $\sigma(E_R) = 0.32\,\mathrm{keV}\sqrt{E_R/\mathrm{keV}}$. This was then converted into the energy resolution for nuclear recoils using a Lindhard model quenching factor [33] with a Lindhard factor of 0.174, as given in [27]. LUX's efficiency is taken directly from Figure 1 in [27], within an energy window $1.1 < E_R < 50\,\mathrm{keV}$.

3.2 Example Recoil Spectra at DEAP-3600 and XENON1T

To illustrate the phenomenology of NDM scattering, we compare the reconstructed recoil spectra of NDM with that of a WIMP in DEAP-3600 and XENON1T. In Figure 1, the recoil energy spectra for a range of k values are shown for each experiment. For each value of k we display the spectra with and without (bold and dashed lines respectively) the inclusion of the detector energy resolution and efficiency as detailed in Section 3.1. We have fixed the NDM model parameters R_1 and m_1 to 1 fm and 1 GeV respectively in analogy with the SM. We have no fundamental guide for what these parameters should be in the dark sector, so we have chosen to take the SM values as a place to start. These parameters will remain fixed at these values throughout the rest of this paper. Also shown in each plot of Figure 1 is the reconstructed recoil spectrum of a standard WIMP with a mass and elastic scattering cross-section per SM nucleon of 100 GeV and 10^{-46} cm^2 respectively. We use a Maxwell-Boltzmann dark matter velocity distribution for the WIMP spectrum and assume the scattering is isotropic and momentum-independent.

In most cases even with detector effects included the oscillations of the k-DN form factor can be seen, which contrasts with the monotonically decreasing WIMP spectrum[2]. The period of the oscillations in the NDM recoil energy spectrum decreases with k, as the size of the k-DN states increase. It is worth noting at this point that the slope enveloping these oscillations also steepens with k, due to the inverse dependence of the form factor on k as shown in Equation (2.1).

Comparison of the solid and dashed curves in Figure 1 demonstrates the effect of the finite experimental energy resolution. The sharpness of the features are smoothed out leading to less significant troughs in the spectrum and simultaneously decreasing the height of the peaks. As k increases the period of the oscillations will decrease and the effect of the energy resolution smearing becomes more prominent. As the oscillation period approaches

[2]The WIMP spectrum will start increasing again due to the oscillations in the SM form factor, but this occurs far beyond the maximum energy window of DEAP-3600 and XENON1T that we consider here.

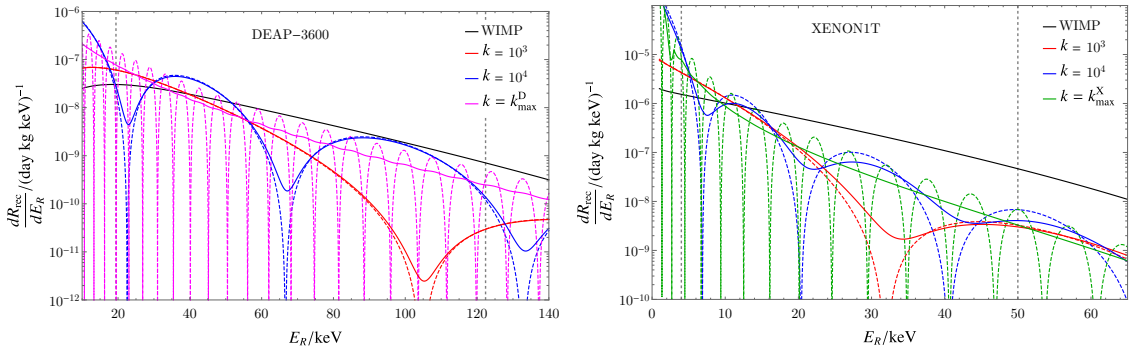

(a) (b)

Figure 1: (a): Comparison of the recoil energy spectra for NDM along with that of a 100 GeV WIMP for DEAP-3600. Spectra are plotted for three different k values: 10^3 (red), 10^4 (blue), and $k^{\rm D}_{\rm max} = 6.5 \times 10^6$ (purple). (b): Comparison of the recoil energy spectra for NDM along with that of a 100 GeV WIMP for XENON1T. Spectra are plotted for three different k values: 10^3 (red), 10^4 (blue), and $k^{\rm X}_{\rm max} = 5.8 \times 10^5$ (green). The bold and dashed lines represent the spectra with and without the finite energy resolution and efficiencies taken into account for each experiment using the experimental parameters in Equation (3.1) and Equation (3.2) for DEAP-3600 and XENON1T respectively. In the NDM cases we have set $R_1 = 1$ fm and $m_1 = 1$ GeV. Vertical dashed lines represent the limits of the energy windows of the two experiments. The WIMP-SM nucleon scattering cross-section was fixed to be 10^{-46} cm^2 and the NDM cross-sections were scaled such that the integrated rates were equal to that of the WIMP across the energy window of each experiment.

the energy resolution of the detector it is clear that there is a value $k_{\rm max}$ beyond which the characteristic oscillations of the form factor can no longer be resolved. In particular, the non-decreasing parts of the spectrum are smoothed away leaving a monotonically decreasing spectrum. This transition is important for our analysis as it represents the value of k beyond which the distinguishability between the NDM spectrum and the WIMP spectrum is no longer determined by the non-decreasing sections of the spectrum but rather by the shape of the slope as a whole. We note that a non-standard velocity distribution may allow a WIMP spectrum to mimic the NDM spectrum for dark nuclei with $k > k_{\rm max}$, while for lower k values the non-decreasing sections of the NDM spectrum would still allow an experiment to distinguish NDM from a WIMP spectrum no-matter what the velocity distribution.

We can determine $k_{\rm max}$ by finding when the period of the oscillations at the threshold energy[3] is approximately equal to the width of the response function, $\sigma(E_R^{\rm th})$, where $E_R^{\rm th}$

[3]We compare at the threshold energy as this is where the dominant part of the signal will come from and is where the period of the oscillation is smallest.

is the threshold energy of the detector. This leads to

$$k_{\rm max} \sim \left(\frac{\pi^2}{4 m_N R_1^2 \left(E_R^{\rm th} - \sqrt{(E_R^{\rm th})^2 - \sigma (E_R^{\rm th})^2} \right)} \right)^{3/2} . \tag{3.3}$$

Beyond $k_{\rm max}$ we expect the dominant part of the NDM spectrum to be effectively a monotonically decreasing function of the recoil energy. In Figure 1, we have plotted the $k_{\rm max}$ for each detector, $k_{\rm max}^{\rm D}$ for DEAP-3600 and $k_{\rm max}^{\rm X}$ for XENON1T, and in each case we can see that the spectra including the detector effects have been smoothed out leaving no rising sections.

Conversely if we decrease the value of k sufficiently we will eventually generate a recoil spectrum that has no rising sections within the energy window of the experiment. The NDM form factor in this region only produces a modification in the slope of the recoil energy spectrum, which again could be mimicked easily by a WIMP spectrum. Defining $k_{\rm min}$ as the DN number at which the first trough in the recoil spectrum enters the energy window, we find

$$k_{\rm min} \sim \left(\frac{4.5}{R_1 \sqrt{2 m_N E_{\rm up}}} \right)^3 , \tag{3.4}$$

where $E_{\rm up}$ is the upper end of the sensitivity energy window for a given experiment. With these definitions, for each experiment there is a range of k values in which the distinctive rising features of the dark form factor may be seen within the energy window of a detector; outside this region we expect NDM spectra to be monotonically decreasing.

For DEAP-3600 this k range is

$$800 \lesssim k \left(\frac{R_1}{1{\rm fm}} \right)^3 \lesssim 6.5 \times 10^6 . \tag{3.5}$$

and for XENON1T the equivalent range is

$$500 \lesssim k \left(\frac{R_1}{1{\rm fm}} \right)^3 \lesssim 5.8 \times 10^5 . \tag{3.6}$$

The lower bound in XENON1T is slightly lower than in DEAP-3600 as the first dip appears within the energy window sooner due to the larger mass of the xenon nucleus, leading to a shorter period in the form factor oscillation. Similarly, comparing DEAP-3600 and XENON1T for $k = 10^3$ and $k = 10^4$ we note that for the same value of k the period of oscillations in the spectra is shorter for XENON1T again due to the larger mass of the xenon nucleus producing a larger value for the momentum transfer, q, for a given recoil energy. In addition for the majority of the relevant range of recoil energies, DEAP-3600 has a better energy resolution potentially allowing it to distinguish (using rising sections of the spectra) dark nuclei with larger k values compared to XENON1T as the transition to a monotonically decreasing spectrum will occur at larger values of k for DEAP-3600.

In Section 4 we perform an analysis to determine the number of signal events required to distinguish the NDM spectrum from that of a WIMP. For k values within the ranges in

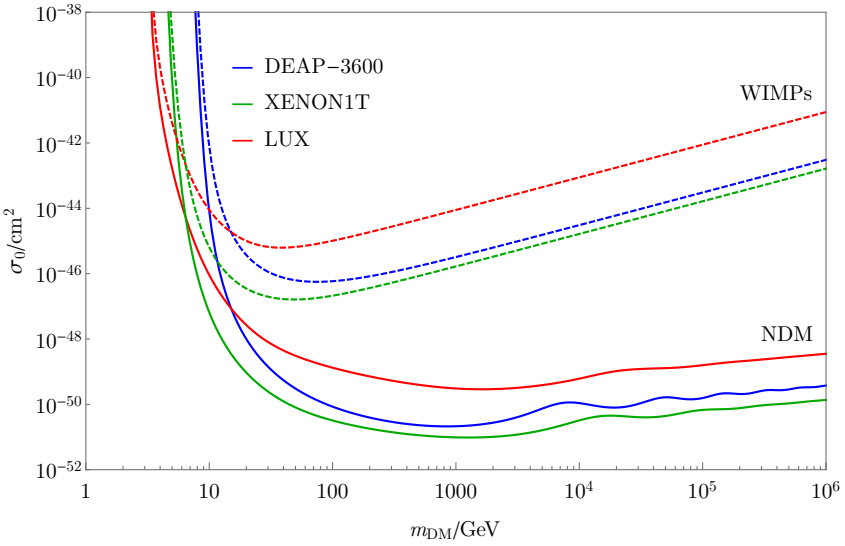

Figure 2: Projected limits at 90% CL for σ_0, the DN-SM nucleon scattering cross-section (in bold), against the dark matter mass for DEAP-3600 (blue) [25] and XENON1T (green) [27], and compared with the strongest current limits from LUX (red) [26]. Also shown are the WIMP limits in the same detectors (dashed lines), where σ_0, is interpreted as the WIMP-SM nucleon scattering cross-section. For the NDM limits we have taken $m_1 = 1$ GeV and $R_1 = 1$ fm.

Equation (3.5) and Equation (3.6) the number of signal events required to identify the NDM spectrum will depend on two main properties; where the first (and sometimes subsequent) rising section of the spectrum appears in the energy window and what the amplitudes of the oscillations are after detector energy resolution has been taken into account.

3.3 Current and Projected Exclusion Limits

While our main focus is to examine whether we can distinguish NDM from WIMP signal events, we finish this section with a discussion of the current and projected limits on models of NDM if neither DEAP-3600 or XENON1T observe any candidate signals. Figure 2 shows the 90% confidence level (CL) limits we calculate on σ_0, the DN-SM nucleon scattering cross-section for NDM, compared with the equivalent limits for a standard WIMP, each as a function of the mass of the dark matter state. For NDM, the mass of the dark matter state is given as $m_k = k\, m_1$, where we have fixed the mass of an individual DN to $m_1 = 1$ GeV. As a result the x-axis is equivalent to the number of DNs, k, for the nuclear states.

In both the NDM and WIMP cases, we show the projected limits for DEAP-3600 and XENON1T and the current limit derived from LUX. All NDM limits are calculated using Equation (2.8) with the requisite detector information from Section 3.1. Our calculated WIMP limits (dashed lines in Figure 2) are in good agreement with the results presented in the experimental papers [25–27].

Comparing the NDM limits with those for WIMPs, from Equation (2.6) we see that the constraint on the DN-SM nucleon cross-section is much stronger than for the WIMP.

In the lower mass region below 100 GeV, the ratio of the NDM and WIMP limits for a given dark matter mass goes approximately as k^2 as in this region the dark form factor is still close to unity. Towards higher masses the dark form factor suppresses the overall rate and therefore weakens the limits. The limiting behaviour of the event rate for large k goes as $\sim k^{-1/3}$ and as a result the elastic scattering cross-section limit for dark nuclei increases as $k^{1/3}$ in contrast to the usual WIMP limit, which increases linearly with $m_{\rm DM}$.

In the high mass region the NDM limits also exhibit oscillations (due to the dark form factor), which are more pronounced in the case of DEAP-3600. These arise because as k (and therefore m_k) increases there are k values for which the experiment energy window contains more peaks than troughs and visa-versa, which results in increased (or decreased) sensitivity. This effect is less pronounced in LUX and XENON1T as the energy resolution is not as good in the high recoil energy region; this means the amplitude of the oscillations in the recoil spectra is not reconstructed as sharply, which results in the flatter limit shape. The scale of the NDM limit largely depends on the overall count rate above the energy threshold *i.e* if DEAP-3600's lower energy threshold could be reduced by a factor of ~ 2, below $\sim$ 8 keV, then it could be more sensitive to NDM in the high mass region than XENON1T.

The overall scale of the limits on the DN-SM nucleon scattering cross-section is several orders of magnitude more restrictive than that for the WIMP case. In the example of a scalar interaction between a SM quark and a DN (scalar or fermion), we can translate the limits from direct detection to an upper limit on the DN annihilation to SM quarks. We find a result that is many orders of magnitude below what is required for achieving the correct abundance via standard freeze-out. This is no great surprise as it has been known for some time [34] that it is very difficult to have a sufficiently large dark matter annihilation rate to SM quarks for asymmetric freeze-out to produce an abundance that is determined by the dark matter asymmetry. The limits from direct detection and mono-jet searches at the LHC rule out the viable parameter regions involving interactions with quarks or gluons. The process of asymmetric freeze-out in NDM models can proceed, however, via the annihilation into lighter hidden sector states [21]. These hidden sector states may also be limited in a model-dependent way by astrophysical constraints, the details of which are beyond the scope of this work.

4 Identifying Nuclear Dark Matter

Perhaps the most interesting question is: if DEAP-3600 or XENON1T do see a candidate signal above the background, how many events are required to identify nuclear dark matter? In this section we calculate the number of events required to distinguish between the NDM and WIMP hypotheses ($N_{\rm req}$) at a given CL.

In the absence of knowledge about the nature of dark matter particles, we compare each NDM spectrum (of varying k values) with the most similar WIMP-induced recoil energy distribution. This most similar WIMP mass can be different for each k, and therefore the number of events required to effectively distinguish between the hypotheses will be different in each case.

We start by finding the WIMP spectrum which is the most indistinguishable, *i.e* requires the highest number of events to distinguish, from each hypothesised NDM spectrum. To this end we define a test statistic, λ, as a negative log likelihood (NLL) ratio;

$$\lambda = -2 \ln \left(\frac{\mathcal{L}_{\text{NDM}}}{\mathcal{L}_{\text{WIMP}}} \right), \tag{4.1}$$

where $\mathcal{L}_{\text{NDM/WIMP}}$ is the likelihood of an event occurring due to a NDM or WIMP dark matter candidate. Here values greater than zero correspond to data sets which are more WIMP-like than NDM-like. An unbinned extended likelihood is used giving

$$\mathcal{L}_{\text{NDM/WIMP}} = \text{Poisson}\left\{N_{\text{obs}}, N_{\text{exp}}(\sigma_0, k, m_1)\right\} \prod_{i=1}^{N_{\text{obs}}} f(E_i|k, m_1). \tag{4.2}$$

where $f(E_i|k, m_1)$ is the reconstructed recoil energy probability density function (PDF) for the WIMP ($k = 1$) or NDM case. The mass m_1 (the mass of a single DN or WIMP, depending on the case), and elastic scattering cross-section σ_0, are allowed to take independent values for the NDM and WIMP cases. The scattering cross-section acts as an overall normalisation factor (under our assumptions of isotropic and velocity-independent scattering) in both distributions; as such, it only appears in the integral number of expected events N_{exp}. The most indistinguishable case occurs when the expected number of events is the same for both NDM and WIMP dark matter, thus the Poisson term can be dropped from the likelihood ratio and only the shape of the distributions is compared.

For each hypothesised number of observed events the probability, p, of misidentifying NDM as WIMPs is determined from the PDF of λ, $g(\lambda|N_{\text{obs}})$, where

$$p = \int_0^{\infty} g(\lambda|N_{\text{obs}}) d\lambda. \tag{4.3}$$

The PDF is built using a Monte Carlo simulation where events are created under the NDM hypothesis for a given k. A confidence level $C = 1 - p$ is then assigned which corresponds to the probability that a dataset will be correctly identified as NDM-like under the NDM hypothesis.

The test was carried out for a range of k values, logarithmically distributed between $k = 10$ and $k = 10^7$, with $m_1 = 1$ GeV. This range accommodates those specified in Equation (3.5) and Equation (3.6), where we expect the non-decreasing sections of the dark form factor to be visible within each detector's energy window. For the WIMP distributions a table was built comprising of 5000 WIMP mass spectra logarithmically distributed between $m = 10$ GeV and $m = 10^6$ GeV. This range accounted for all possible WIMP distribution shapes. When k is small, we do not expect dark form factor effects to be significant, and therefore the most indistinguishable WIMP will likely have around the same mass as the k-DN state. This means WIMP spectra of masses below 10 GeV will not be relevant. Furthermore, the sensitivity of DEAP-3600 and XENON1T sharply falls below this mass (see Figure 2), and so the potential for detection is greatly reduced. For WIMPs of mass 10^6 GeV or greater, the spectra are indistinguishable (in shape) from each other, and so do not affect the analysis which is only shape-dependent.

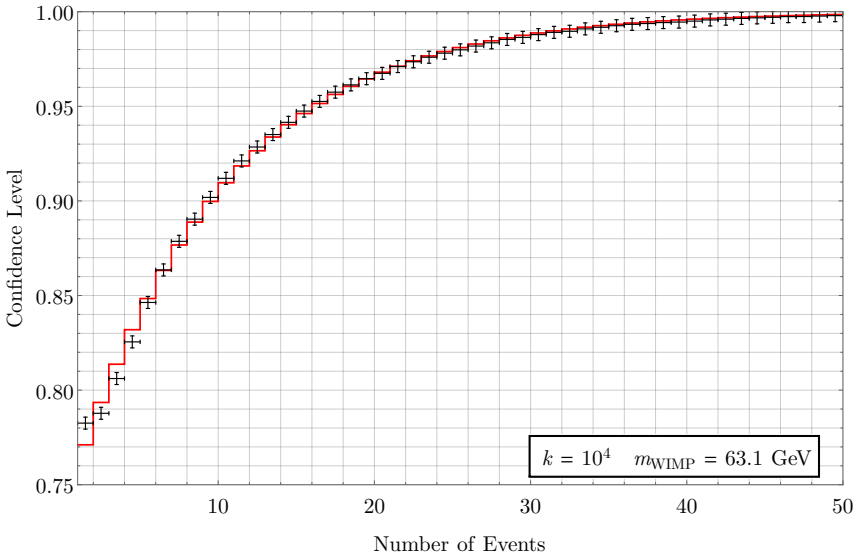

Figure 3: The CL for each value of N_{obs} up to $N_{\mathrm{obs}} = 50$ for $k = 10^4$ ($m_1 = 1\,\mathrm{GeV}$) compared to a 63.1 GeV WIMP. The black crosses mark the values found from the Monte Carlo simulation, while the red line presents Equation (4.4) when fitted to this data. The integer number of events ($\lfloor N_{\mathrm{obs}} \rfloor$) is used in Equation (4.4), which is reflected in the equation's step-like shape.

The WIMP spectra table was scanned through for each value of k. The number of events required to distinguish between the NDM and WIMP hypotheses up to a 3 σ CL was then determined for each WIMP mass. Generating adequate Monte-Carlo statistics to produce distributions of $g(\lambda|N_{\mathrm{obs}})$ for each of the masses and number of events is computationally expensive. Consequently, 10^5 pseudo-experiments were used for all potential WIMP spectra and the distribution of CLs was determined by fitting a modified non-central chi-squared cumulative distribution function (CDF):

$$C(N_{\mathrm{obs}}) = 1 - Q_{\frac{a}{2}}\left(\sqrt{b}, \sqrt{\frac{N_{\mathrm{obs}}}{c}}\right), \tag{4.4}$$

where $Q_{\frac{a}{2}}$ is the Marcum Q-function. Here the parameters a, b, and c are left as variables in the fit.

This function fits well to all CL distributions, one of which is illustrated in Figure 3. The CL is shown for each value of N_{obs} up to $N_{\mathrm{obs}} = 50$ for $k = 10^4$ ($m_1 = 1\,\mathrm{GeV}$) compared to a 63.1 GeV WIMP (the most indistinguishable). Equation (4.4) was fitted to these points with the inverse being used to determine the number of events required for each CL. Here excellent agreement is seen between the Monte Carlo data and the fit, supporting the use of Equation (4.4) in the analysis.

Figure 4 shows a selection of NDM spectra as reconstructed by DEAP-3600, which are plotted across the energy window of the detector. In each sub-figure the spectrum is plotted alongside that of the most indistinguishable WIMP at that k value. The top left

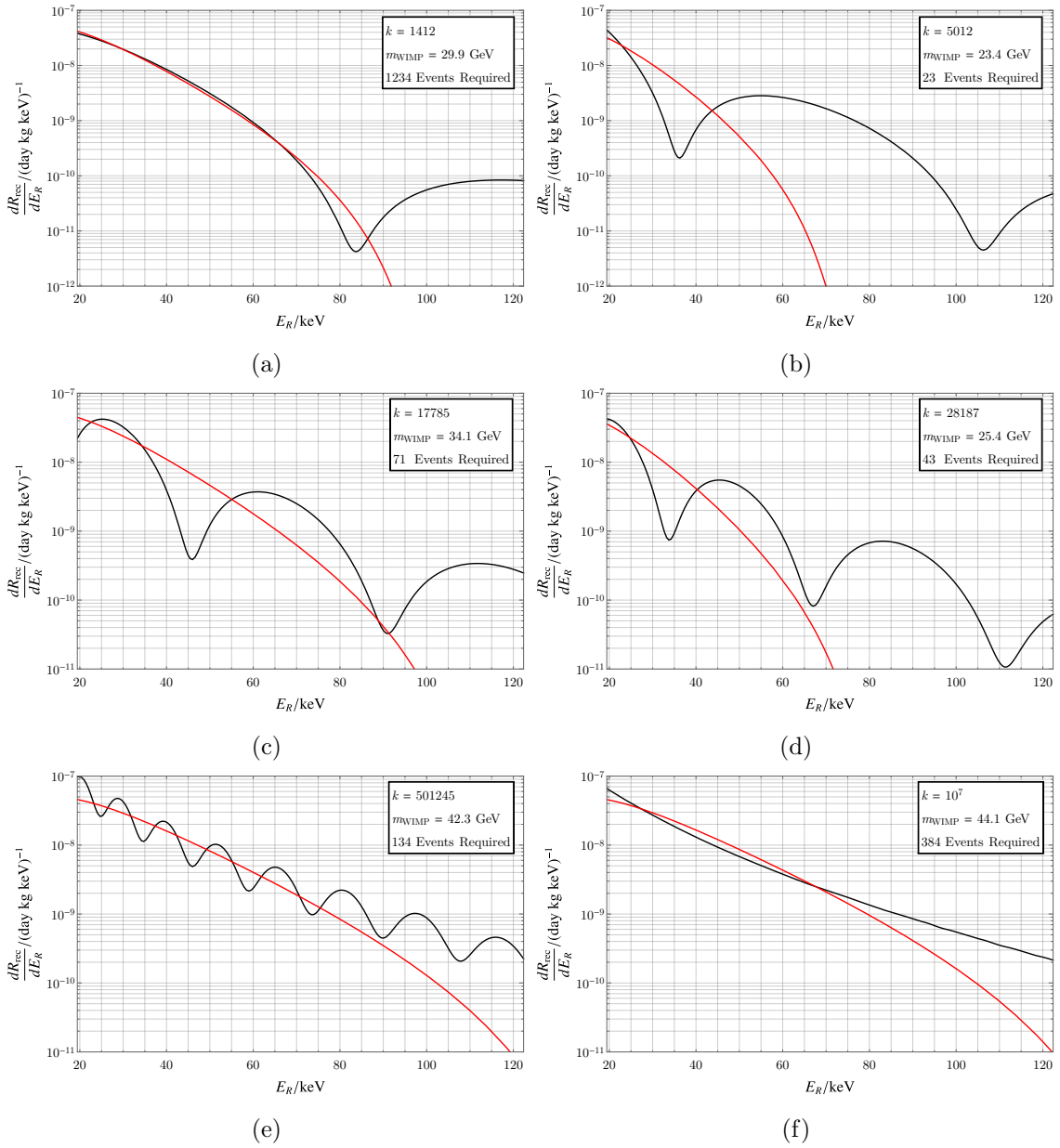

Figure 4: Example NDM spectra (black) along with the most indistinguishable WIMP spectra (red), as reconstructed by DEAP-3600. Inset into each plot is the k value, the mass of the best fitting WIMP (m_{WIMP}), and the number of events required to distinguish between the spectra to a $3\,\sigma$ CL.

panel (Figure 4a) shows the spectra for $k = 1412$, which is the first bin in the k range in Figure 5, where the number of events required to distinguish up to a $3\,\sigma$ CL is plotted as a function of k, for DEAP-3600 (above) and XENON1T (below). In the $k = 1412$ case, the first trough in the recoil spectrum has just entered into the energy window, and the WIMP spectrum closely matches that of NDM. Subsequently the number of events

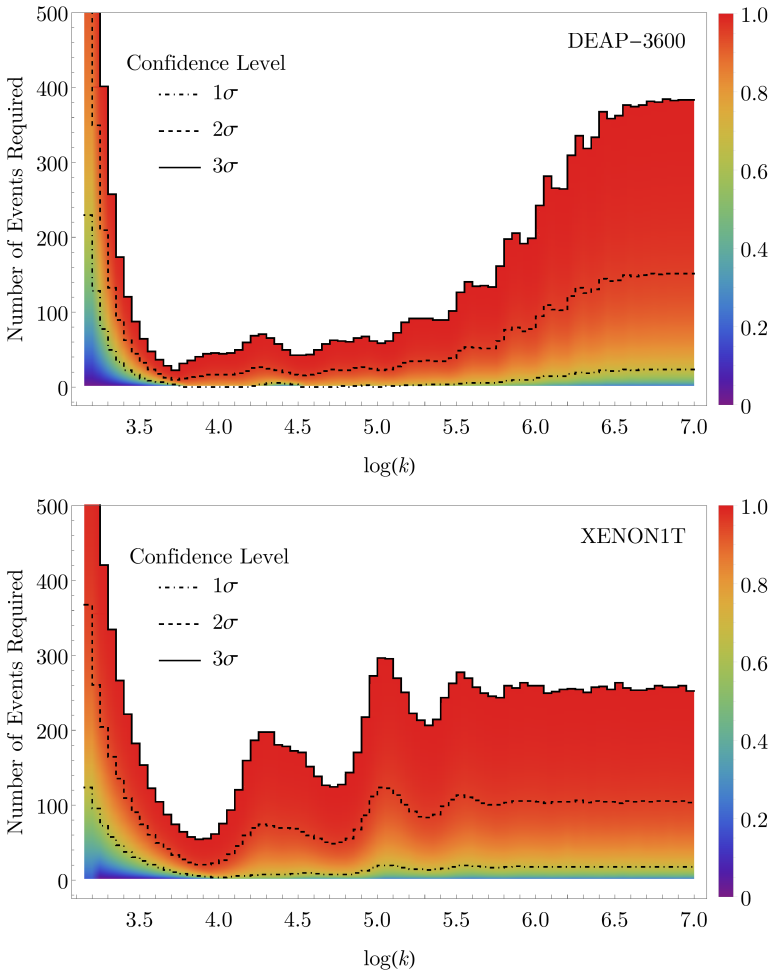

Figure 5: The number of events required to distinguish between values of k and all WIMP masses to the stated CL in DEAP-3600 (above) and XENON1T (below). Here the CL given by Equation (4.4) is shown by the colour scale with 1, 2, & 3 σ shown as dot-dashed, dashed, and solid lines respectively.

required to distinguish to 3 σ is large (1234). As k drops below this value, N_{req} gets larger and eventually the first trough leaves the energy window with distinguishability between WIMP and NDM spectra becoming effectively impossible. In the event of a signal in this case, one could only put an upper limit on k.

In Figure 4b (top right panel) where $k = 5012$, the first trough occurs at a lower recoil energy, and the WIMP spectrum no longer closely follows that of NDM. Here, the relative contribution of the second peak is much greater than in Figure 4a, by around a factor of 100. Given that N_{req} decreases by approximately this factor as well, this suggests the rise in the spectrum, which is irreproducible with a standard WIMP, acts as the dominant distinguishing feature of the spectra. This claim is further supported when we notice that N_{req} in each of these cases is just enough to be able to resolve the second peak (and

consequently, the first trough)[4]. Only 23 events are required in the case that $k = 5012$, which corresponds to the lowest value across the entire range for DEAP-3600, *i.e* the deepest minimum in Figure 5.

This distinguishing mechanism is also at work in the case that $k = 17785$ (seen in Figure 4c, the middle left panel), which corresponds to the first peak following the central minimum at $k = 5012$ in Figure 5. Here the threshold is just at the beginning of a peak, which means the NDM spectrum follows the WIMP spectrum more closely than in the previous case and the second peak occurs later on, subsequently N_{req} is larger.

The next minimum in N_{req} lies at $k = 28187$, whose spectrum is seen in Figure 4d (middle right panel). Here the threshold intersects the oscillations approximately as it does in Figure 4b for $k = 5012$, however more events are required to distinguish in the $k = 28187$ case. This reflects the effect of the finite energy resolution which smears out the troughs, reducing their depth and making them less distinctive.

It is clear now that as k is increased, N_{req} oscillates as the spectra change between configurations such as those in Figure 4b & 4d, and that in Figure 4c. These fluctuations are seen in Figure 5 for both DEAP-3600 and XENON1T, the difference between them will be discussed later. The ability to distinguish between hypotheses for a particular value of k in this region is dependent on the chosen energy window. If we were to change the lower threshold of the window, this would change the relative size of the second peak and therefore N_{req}. The overall effect of this would be a phase change in the oscillations seen in Figure 5; the troughs and peaks would shift, but their amplitude would not change much. Changing the upper threshold by small amounts will have little effect, as the relative rate in this region is negligible (compared with the rate at threshold).

Inspecting Figure 4e (bottom left panel), where $k = 501245$, which lies in the upwards trending region of Figure 5, we can see the period of the oscillations is much smaller, and the fluctuations have been smeared out significantly. With only $\mathcal{O}(10)$ events, several oscillations in the spectrum can now be probed (as opposed to only the first), however their amplitude has been reduced to such an extent that 134 events are required to distinguish to $3\,\sigma$. The upwards rise in Figure 5 reflects the increase in smearing making distinction harder.

In the last case seen in Figure 4f (bottom right panel) where $k = 10^7$, the oscillations in the NDM spectrum are no longer visible, as their period is too small to be resolved by DEAP-3600. The shape of the slope is still distinct from all WIMP spectra, and so can still be distinguished. However this is under the assumption that the WIMP's velocity is described by a Maxwell-Boltzmann distribution. By considering an alternative velocity distribution, a WIMP spectrum could mimic that of NDM's seen here. Past the point where the oscillations are no longer resolved, the shape of NDM spectra is fixed, and so N_{req} plateaus, as seen in Figure 5.

What one notices across the selection of spectra presented in Figure 4 is that the mass of the most indistinguishable WIMP, m_{WIMP}, approximately follows N_{req}. When N_{req} is

[4] A crude criterion for a resolvable spectral feature is as follows: if the rate in the vicinity of the feature is a factor of $1/N$ smaller than the peak rate within the entire energy window, then at least N events will be needed before events appear in this region, allowing it to be "resolvable".

smaller, so is m_{WIMP} as the NDM spectra start with sharp declines, which WIMP spectra best mimic by decreasing more quickly as well; this trend is created by decreasing the WIMP mass, which causes the distribution of recoil energies to drop off faster.

Comparing DEAP-3600 and XENON1T in Figure 5 one notices the range of k values where distinguishing could be possible (before the plateau region and after the divergence at low k) is greater for DEAP-3600, where N_{req} is also smaller. Both these qualities reflect the benefit of having a better energy resolution when searching for NDM. Furthermore the range of distinguishable k values seen in these plots is in good agreement with the those predicted earlier: Equation (3.5) and Equation (3.6) for DEAP-3600 and XENON1T respectively.

The oscillations in N_{req} have a larger period for XENON1T, which is counter-intuitive given that the period of the recoil spectra's oscillations is smaller. This is a result of the energy threshold being lower; as k increases the dips in the recoil spectrum contract towards the origin, and so get "bunched" around it. This means that by having a lower threshold, troughs will pass through this boundary at a slower pace with increasing k, and so the period of the oscillations in N_{req} increases.

As discussed, the minimum number of events required to distinguish to $3\,\sigma$ in DEAP-3600 is 23, which occurs when $k \sim 5000$. For XENON1T, the minimum is 55 events (as the energy resolution is worse), which occurs when $k \sim 8000$. As the position of the first trough in the recoil spectrum is at lower E_R in XENON1T, one might expect to find this global minimum at a lower k value than in DEAP-3600. However because the energy threshold is also lower, the relative differences are such that the minimum is pushed higher.

The final significant difference one notices between detectors, is the size of N_{req} in the plateau region, which is lower for XENON1T. While the characteristic troughs are not resolved here, the NDM spectra have different slopes. In the case of XENON1T, the slope is sharper and more easily distinguished as the target nuclei are larger.

4.1 Distributions of Nuclear Dark Matter Masses

As mentioned above the generation of NDM may result in a spectrum of k values rather than all DM states having the same number of dark nucleons. A preliminary study was performed to determine the effect of such a spectrum and the impact it has on our ability to reject the WIMP hypothesis. Spectra following a gaussian distributions of k were chosen with varying widths each centred around $k = 5012$. This corresponds to the most distinguishable case for the DEAP-3600 experiment in the examples tested above so will constitute a best case scenario for when we include a spectrum. Figure 6 shows the number of events required to reject the most indistinguishable WIMP hypothesis at a $3\,\sigma$ confidence level as a function of the gaussian width. Here the number of events required for a 1 % width is 25, close to the delta function value of 23 for k=5012. With increasing width the composite spectrum smoothes out, as shown in Figure 7, until a plateau region is reached in the number of required events. This is equivalent to the plateau region observed for high k values in Figure 5 where features in the NDM spectrum are unresolvable by the detector. A delta function centred around k=5012 corresponds to our best case scenario. From here

we find moving to a gaussian distribution, with a width of 100%, increases the number of events required by an order of magnitude.

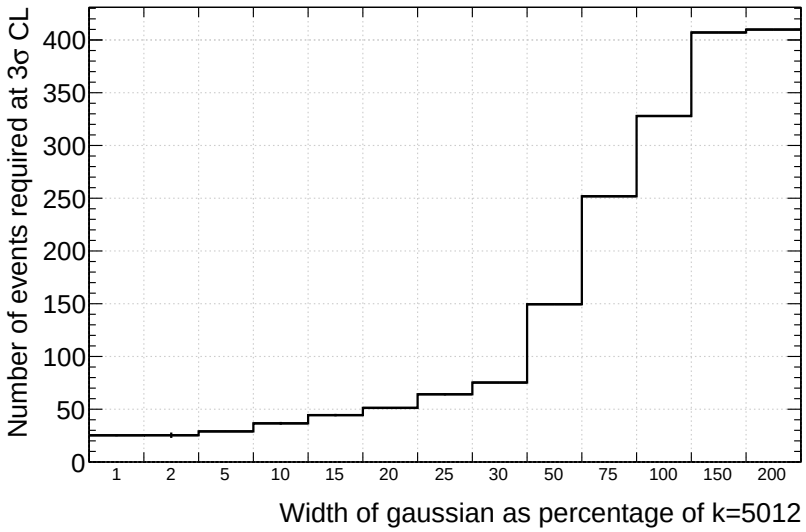

Figure 6: The number of events required to reject the most indistinguishable WIMP hypothesis at a $3\,\sigma$ confidence level versus the width of the gaussian distribution of k values as a percentage of the mean. Here the number of events required for a 1 % width is 25, close to the delta function value of 23 for k=5012. As the width of the distribution of k values increases the composite NDM spectrum smoothes out until a plateau region in the number of events occurs above a width of 200%. This is equivalent to the plateau region observed for high k values in Figure 5.

4.2 Discovery Potential

Finally, we compare the largest number of events ($N_{\rm max}$) that could be seen between NDM and WIMP dark matter, in the tonne-scale experiments coming online now. This is estimated by taking the cross-section to be the LUX limit. Figure 8 shows $N_{\rm max}$ vs. mass for both NDM and WIMPs in the DEAP-3600 and XENON1T experiments, as well as the $N_{\rm req}$ values at 1, 2, & $3\,\sigma$ CLs. For both WIMPs and NDM, $N_{\rm max}$ goes to zero at low mass, where the LUX energy threshold is lower than the relatively conservative projections from DEAP-3600 and XENON1T. The predicted $N_{\rm max}$ rises as the experiments increase in sensitivity relative to the current bound for both NDM and WIMPs, however the two models diverge around 100 GeV, where the value plateaus at $\sim$ 45 (80) events for WIMPs, but oscillates around $\sim$ 20 (60) for NDM in DEAP-3600 (XENON1T). These oscillations occur for the same reason as those in the σ_0 limit in Figure 2; *i.e* the energy window is enclosing varying configurations of the recoil spectra, which results in a fluctuating $N_{\rm max}$.

Comparing $N_{\rm max}$ to $N_{\rm req}$ for NDM, we see that in this scenario there are ranges of $m_{\rm DM}$ where distinguishing to $1\,\sigma$ - $2\,\sigma$ CL could be possible in the current tonne-scale

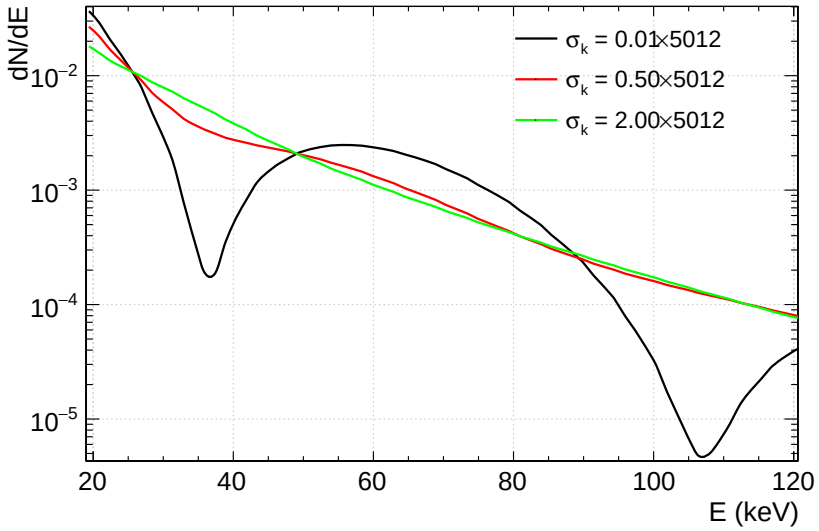

Figure 7: Examples of NDM spectra composed of gaussian distributions of k values with a mean of $k = 5012$ and widths, σ_k, of 1 % (black), 50 % (red), and 200 % (green) of the mean. As the width of the gaussian distribution increases features of the NDM spectrum get washed out resulting in spectra which resemble those of a high k delta function.

experiments individually. This conclusion is most sensitive to the energy threshold and resolution assumed for each experiment in this study.

Throughout our analysis we have set $m_1 = 1$ GeV and $R_1 = 1$ fm. If we were to change these values, we do not expect the discovery potential to change, *i.e* distinguishing to $3\,\sigma$ or over will still not be possible, at least in the high mass region ($m_k \gtrsim 30$ GeV). Instead we expect changes in m_1 and R_1 to expand or contract $N_{\rm req}$ and $N_{\rm max}$ equivalently in Figure 8, and so their values relative to each other do not alter.

In the high mass region m_1 does not effect $g(v_{\rm min})$ significantly and so only scales the scattering rate linearly due to the changes in the number density. Since $N_{\rm req}$ only depends on the relative shape of WIMP and NDM spectra, it is unchanged by varying m_1. Similarly $N_{\rm max}$ is not affected as even though the LUX limit changes (by a factor of m_1), the scattering rate in DEAP-3600 and XENON1T changes by $1/m_1$. Therefore changes to m_1 will not affect the discovery potential in the high mass region. The same can be said of any factor which simply scales the scattering rates.

Varying R_1 changes the size of the k-DN state, R_k, which affects the scattering rate via the dark form factor, so the configuration of oscillations would alter. However this would be equivalent to varying k as this also changes R_k. Varying k also affects m_k (which R_1 does not), but as mentioned above, such a normalisation factor is irrelevant to the discovery potential. Therefore, shifting R_1 or m_1 will simply stretch or contract $N_{\rm max}$ and $N_{\rm req}$ equivalently along the mass axis in Figure 8. The situation is more complex in the lower mass region where changes to $g(v_{\rm min})$ must also be taken into account.

Combining the results from DEAP-3600 and XENON1T would give increased sensitiv-

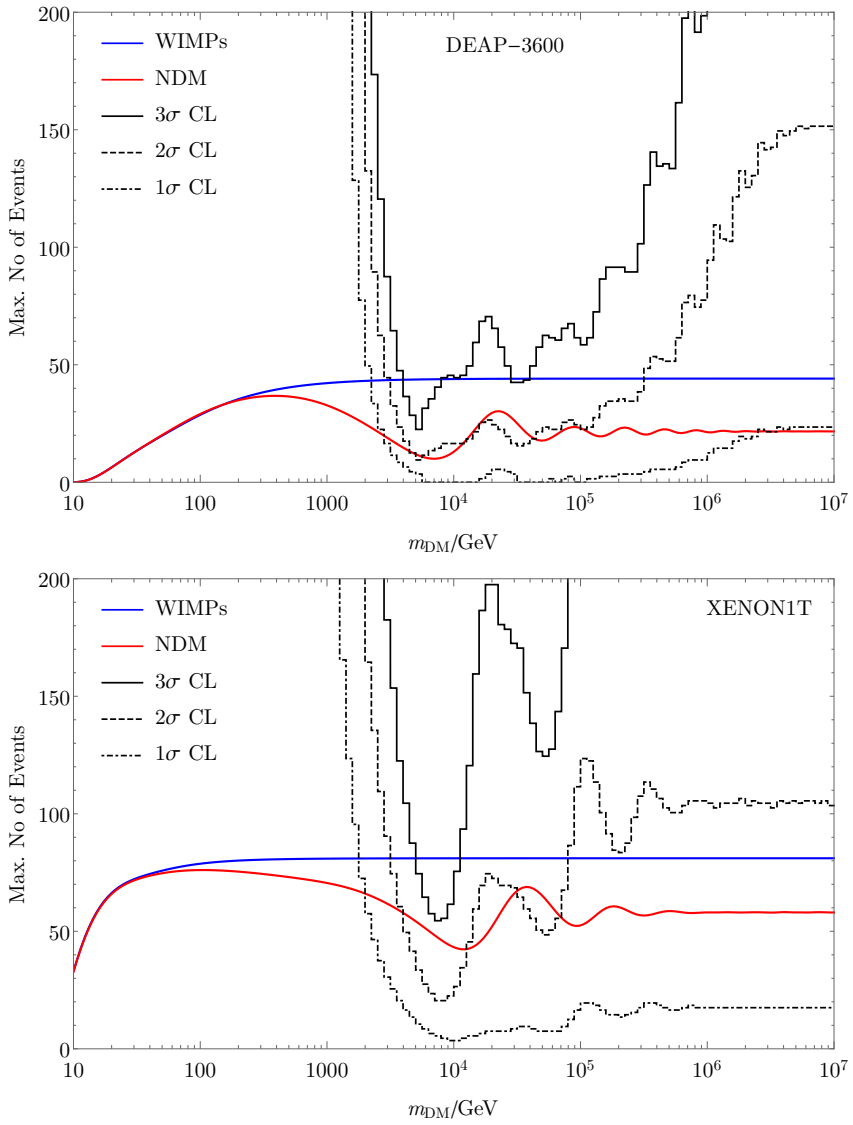

Figure 8: The maximum number of events that could be seen at DEAP-3600 (above) and XENON1T (below) against dark matter mass for NDM (red) and WIMPs (blue), plotted alongside the 1, 2, & 3 σ CL lines (the dot-dashed, dashed, and bold lines respectively) for distinction as seen in Figure 5.

ity to NDM for a range of parameter space, roughly from $3.8 < \log(k) < 4.8$. To estimate this, we combine the misidentification probabilities from Equation (4.3) to find an overall probability C_{comb} of positively identifying NDM in at least one detector, *i.e*

$$C_{\text{comb}} = 1 - p_{\text{D}} p_{\text{X}}. \tag{4.5}$$

Figure 9 shows the result of this for total numbers of events seen across both detectors. The fractional contribution to the total from each experiment is calculated from the expected number of events over each of the detectors' nominal run times. The number of events

required is plotted with the total maximum number of events which shows two regions in the range from $3.8 < \log(k) < 4.8$ where there is a $3\,\sigma$ CL of distinguishing NDM from WIMP dark matter.

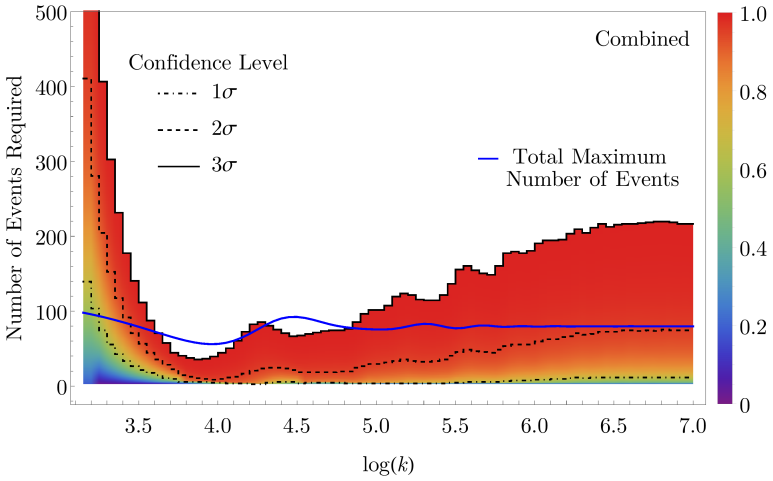

Figure 9: The number of events required to positively identify NDM at a given CL with DEAP-3600 and XENON1T combined. The total maximum number of events from both experiments (blue line) reveals two regions of k which can be positively identified as NDM at a $3\,\sigma$ confidence level.

While $2\,\sigma$ "hints" of NDM could be seen in the individual tonne-scale experiments coming online now, and $3\,\sigma$ level is achievable over a moderate range of parameter space by combining results, larger follow-on detectors under consideration would have significantly enhanced sensitivity. Here we make a simple estimate of the sensitivity for argon (20T) and xenon (7T) targets, since such detectors have been recently proposed or are in the development stage. Taking a 20T argon detector's specifications (the efficiency, etc.) to be the same as DEAP-3600's, then $N_{\max}$ in Figure 8 can simply be scaled for the follow-on detector. Thus we can expect $N_{\max}$ in this detector to oscillate around 400 events with a peak of 800, which is enough to distinguish the entire k range to at least $3\,\sigma$ where it is possible to do so. Making the same estimate for a 7T xenon detector with the same specifications as XENON1T, we can expect $N_{\max}$ also to oscillate around 400 events with a peak of 650, which similarly distinguishes NDM from WIMPs to at least $3\,\sigma$. These extrapolations are conservative estimates, as better efficiency, energy thresholds, and so forth, are to be expected.

The outlook for searches for NDM in DEAP-3600 and XENON1T is much the same: distinguishing NDM spectra to $2\,\sigma$ CL is possible in both, individually. While the number of events required to distinguish is lower in DEAP-3600, as it has better energy resolution and oscillations in the recoil spectra have smaller periodicity, XENON1T benefits from a reduced lower energy threshold which pushes the sensitivity higher. An ideal detector for probing NDM would optimise for the lowest possible energy resolution, and preferably have

a liquid argon target to access the broadest range of k values, as long as the lower energy threshold could be sufficiently small.

5 Discussion and Conclusion

Typically dark matter models assume dark matter is a point-like particle, however composite dark matter forming spatially-extended bound states is an area of increasing interest. If dark matter is composite, it will have unique phenomenology in direct detection searches, which often provide our most stringent dark matter bounds. This paper studies the signals of NDM, following [21], in the tonne-scale argon and xenon experiments coming online now, DEAP-3600 and XENON1T respectively.

The model considered in this paper is motivated by SM nuclear physics with composite dark matter states consisting of DNs bound together under an analogous strong nuclear force. A striking feature of this class of model is the oscillations in the dark form factors, which may be seen in the tonne-scale direct detection searches, when realistic detector energy response, thresholds, and resolutions are taken into account.

We find predicted limits on benchmarks cases of NDM assuming no events are seen by DEAP-3600 or XENON1T, along with those inferred from the null result from LUX. The limits on σ_0, the DN-SM nucleon scattering cross-section, are orders of magnitude below the equivalent WIMP limits, owing to a k^2 enhancement arising in the scattering rate. The projected limits on WIMP and NDM scattering cross-sections are found to be slightly stronger in XENON1T than in DEAP-3600. The benefit of argon over xenon targets in the high mass region is reduced as the lower energy threshold is higher and so DEAP-3600 is probing deeper into the dark form factor where the rate is suppressed. However if DEAP-3600's lower energy threshold were lowered to ~ 8 keV, then it would be more sensitive than XENON1T to NDM in the high mass region.

Likelihood tests were carried out to determine how many events DEAP-3600 and XENON1T would need to detect in order to distinguish between WIMP and NDM spectra. The number of required events for each value of k was found to be dependent on the detector energy threshold, which determines the relative contribution of the second NDM peak in the energy window, and the energy resolution, which determines the amplitude of the characteristic oscillatory features.

The lowest number of events required for the same level of distinction was found to be 23 events in DEAP-3600 and 55 in XENON1T, which occurs for $k \sim 5000$ and ~ 8000 respectively. After this point, the required number of events oscillates with k as the configurations of the recoil spectra in the energy window vary. These fluctuations reflect the relative difficulty of resolving the second peak in the energy window, which is the dominant distinguishing feature.

Setting the DM elastic scattering cross-section to the limit derived from LUX, the maximum number of events which could be seen in DEAP-3600 and XENON1T was derived and found to oscillate around 20 and 60 respectively. While this is likely to be only enough to see "hints" of NDM in individual detectors, combining results can reach $3\,\sigma$ over a range

of k values, and future upgrades to both detectors would be able to distinguish NDM from a WIMP to $3\,\sigma$ over the entire k range considered.

In this analysis we have compared the detection of NDM of a single size to a WIMP with a decaying exponential recoil spectrum. As outlined in the introduction, the choice of NDM model was driven by the unique spectral features produced by the single dark form factor. An extension to this analysis would be to consider the recoil spectrum produced by a distribution over dark nuclei sizes. The resulting recoil shape no longer contains non-decreasing sections and by exploiting the uncertainty in the DM velocity distribution, a WIMP recoil spectrum could easily mimic this NDM spectrum in a single detector. An obvious extension to this work therefore is to consider a multi-target halo-independent analysis to distinguish between NDM with a distribution of nuclear sizes and WIMP DM.

On the WIMP side we have considered a DM state which generates a decaying exponential recoil spectrum. We note that models of WIMP DM can include interactions that are momentum dependent and this momentum dependence can lead to features in the recoil spectrum, in particular non-decreasing sections at low recoil energies [35]. Such a spectrum would be much more challenging to distinguish from the NDM spectra considered in this paper and is an analysis that is worth pursuing in future work.

Acknowledgements

We acknowledge support from the Science and Technology Facilities Council (grant number ST/L000512/1).

References

[1] **Planck** Collaboration, P. A. R. Ade et al., *Planck 2015 results. XIII. Cosmological parameters*, arXiv:1502.01589.

[2] M. Pospelov and A. Ritz, *Astrophysical Signatures of Secluded Dark Matter*, *Phys.Lett.* **B671** (2009) 391–397, [arXiv:0810.1502].

[3] J. D. March-Russell and S. M. West, *WIMPonium and Boost Factors for Indirect Dark Matter Detection*, *Phys.Lett.* **B676** (2009) 133–139, [arXiv:0812.0559].

[4] W. Shepherd, T. M. Tait, and G. Zaharijas, *Bound states of weakly interacting dark matter*, *Phys.Rev.* **D79** (2009) 055022, [arXiv:0901.2125].

[5] R. Laha and E. Braaten, *Direct detection of dark matter in universal bound states*, *Phys.Rev.* **D89** (2014), no. 10 103510, [arXiv:1311.6386].

[6] R. Laha, *Directional detection of dark matter in universal bound states*, *Phys. Rev.* **D92** (2015), no. 8 083509, [arXiv:1505.02772].

[7] H. M. Hodges, *Mirror baryons as the dark matter*, *Phys. Rev.* **D47** (1993) 456–459.

[8] H. Goldberg and L. J. Hall, *A New Candidate for Dark Matter*, *Phys. Lett.* **B174** (1986) 151. [,467(1986)].

[9] Z. G. Berezhiani and R. N. Mohapatra, *Reconciling present neutrino puzzles: Sterile neutrinos as mirror neutrinos*, *Phys. Rev.* **D52** (1995) 6607–6611, [hep-ph/9505385].

[10] Z. G. Berezhiani, A. D. Dolgov, and R. N. Mohapatra, *Asymmetric inflationary reheating and the nature of mirror universe*, *Phys. Lett.* **B375** (1996) 26–36, [hep-ph/9511221].

[11] R. Foot and R. R. Volkas, *Neutrino physics and the mirror world: How exact parity symmetry explains the solar neutrino deficit, the atmospheric neutrino anomaly and the LSND experiment*, *Phys. Rev.* **D52** (1995) 6595–6606, [hep-ph/9505359].

[12] R. N. Mohapatra and V. L. Teplitz, *Mirror dark matter and galaxy core densities of galaxies*, *Phys. Rev.* **D62** (2000) 063506, [astro-ph/0001362].

[13] R. Foot, *Mirror matter-type dark matter*, *Int. J. Mod. Phys.* **D13** (2004) 2161–2192, [astro-ph/0407623].

[14] D. E. Kaplan, G. Z. Krnjaic, K. R. Rehermann, and C. M. Wells, *Atomic Dark Matter*, *JCAP* **1005** (2010) 021, [arXiv:0909.0753].

[15] J. M. Cline, Z. Liu, G. Moore, and W. Xue, *Scattering properties of dark atoms and molecules*, *Phys. Rev.* **D89** (2014), no. 4 043514, [arXiv:1311.6468].

[16] J. M. Cline, Z. Liu, G. Moore, and W. Xue, *Composite strongly interacting dark matter*, *Phys. Rev.* **D90** (2014), no. 1 015023, [arXiv:1312.3325].

[17] G. Krnjaic and K. Sigurdson, *Big Bang Darkleosynthesis*, arXiv:1406.1171.

[18] W. Detmold, M. McCullough, and A. Pochinsky, *Dark Nuclei I: Cosmology and Indirect Detection*, arXiv:1406.2276.

[19] M. B. Wise and Y. Zhang, *Stable Bound States of Asymmetric Dark Matter*, *Phys. Rev.* **D90** (2014), no. 5 055030, [arXiv:1407.4121]. [Erratum: Phys. Rev.D91,no.3,039907(2015)].

[20] M. B. Wise and Y. Zhang, *Yukawa Bound States of a Large Number of Fermions*, *JHEP* **02** (2015) 023, [arXiv:1411.1772].

[21] E. Hardy, R. Lasenby, J. March-Russell, and S. M. West, *Big Bang Synthesis of Nuclear Dark Matter*, *JHEP* **06** (2015) 011, [arXiv:1411.3739].

[22] E. Hardy, R. Lasenby, J. March-Russell, and S. M. West, *Signatures of Large Composite Dark Matter States*, *JHEP* **07** (2015) 133, [arXiv:1504.05419].

[23] G. Gelmini, A. Kusenko, and S. Nussinov, *Experimental identification of nonpointlike dark matter candidates*, *Phys. Rev. Lett.* **89** (2002) 101302, [hep-ph/0203179].

[24] J. F. Cherry, M. T. Frandsen, and I. M. Shoemaker, *Halo Independent Direct Detection of Momentum-Dependent Dark Matter*, *JCAP* **1410** (2014), no. 10 022, [arXiv:1405.1420].

[25] P. A. Amaudruz et al., *DEAP-3600 Dark Matter Search*, in *International Conference on High Energy Physics 2014 (ICHEP 2014) Valencia, Spain, July 2-9, 2014*, 2014. arXiv:1410.7673.

[26] **XENON** Collaboration, E. Aprile et al., *Physics reach of the XENON1T dark matter experiment*, *JCAP* **1604** (2016), no. 04 027, [arXiv:1512.07501].

[27] **LUX** Collaboration, D. S. Akerib et al., *Improved Limits on Scattering of Weakly Interacting Massive Particles from Reanalysis of 2013 LUX Data*, *Phys. Rev. Lett.* **116** (2016), no. 16 161301, [arXiv:1512.03506].

[28] R. H. Helm, *Inelastic and Elastic Scattering of 187-Mev Electrons from Selected Even-Even Nuclei*, *Phys. Rev.* **104** (1956) 1466–1475.

[29] J. Lewin and P. Smith, *Review of mathematics, numerical factors, and corrections for dark matter experiments based on elastic nuclear recoil*, *Astropart.Phys.* **6** (1996) 87–112.

[30] M. Selvi. Private Communications.

[31] **LUX** Collaboration, D. S. Akerib et al., *First results from the LUX dark matter experiment at the Sanford Underground Research Facility*, *Phys. Rev. Lett.* **112** (2014) 091303, [arXiv:1310.8214].

[32] **LUX** Collaboration, D. S. Akerib et al., *Tritium calibration of the LUX dark matter experiment*, *Phys. Rev.* **D93** (2016), no. 7 072009, [arXiv:1512.03133].

[33] J. Lindhard, V. Nielsen, M. Scharff, and P. V. Thomsen, *Integral Equations Governing Radiation Effects*, *Kong.Dan.Vid.Sel.Mat.Fys.Med.* **33** (1963), no. 10 1–42.

[34] J. March-Russell, J. Unwin, and S. M. West, *Closing in on Asymmetric Dark Matter I: Model independent limits for interactions with quarks*, *JHEP* **08** (2012) 029, [arXiv:1203.4854].

[35] S. Chang, A. Pierce, and N. Weiner, *Momentum Dependent Dark Matter Scattering*, *JCAP* **1001** (2010) 006, [arXiv:0908.3192].